Special Issue on Advanced Technologies of Motor Drives for Net-Zero Emission

Adaptive Linear Predictive Deadbeat Control Against Machine Parameter Uncertainty of SPMSM Drives for Electric Vehicles

Chao Zhang, Dong Wang, Kaiyuan Lu

***Abstract*—A fast and accurate torque/current response is important for optimizing the efficiency of electric vehicles and promptly implementing braking instructions in emergencies. Deadbeat predictive control has attracted much attention in electrical drives for electric vehicles due to its excellent dynamic performance. However, parameter mismatch significantly influences the performance of conventional deadbeat predictive controllers. Existing solutions can effectively suppress the steady-state error caused by parameter mismatch, but their abilities to improve transient performance against parameter uncertainty are limited. To address this issue, an adaptive linear predictive current deadbeat controller for SPMSM drives is proposed in this manuscript. The actual current response characteristic is first tested by applying a test voltage vector. Thereafter, the final required voltage command, which can bring the current to its new reference, is determined by utilizing the actual machine current response characteristic derived from the test voltage vector. The proposed method is simple to implement and can be combined with many advanced methods to achieve both satisfactory dynamic and steady-state performances against parameter uncertainty. The effectiveness and compatibility of the proposed method have been verified by comparing it with other two advanced deadbeat predictive control methods under different dynamic and parameter mismatch conditions.**

***Index Terms*—Permanent magnet synchronous motor, dynamic response, deadbeat predictive current control, parameter mismatch, adaptive linear prediction.**

I. INTRODUCTION

ELECTRIC vehicles (EVs) have attracted much attention due to their potential to save fossil fuels and reduce greenhouse gas emissions. To reduce energy consumption and increase the cruising range of EVs, many scholars are focusing on improving the energy utilization of the drive system by fast and optimized torque distribution [1]. The fast and accurate torque or torque-producing-current response without large overshoot and variations is the basis for implementing the torque distribution optimization strategy. Moreover, fast and accurate current control will increase the bandwidth of current control loop, which enables fast online searching of optimal operation points, such as maximum-torque-per-ampere (MTPA) [2], [3] or maximum-power-per-ampere (MPPA) [4] operation, where high frequency variation terms are generally injected to find the critical point of the response. In addition, the fast response of torque can also enhance the acceleration and deceleration of EVs, enabling quick starting and braking, which is necessary in urban driving conditions that require frequent starts and stops. In some emergencies, the rapid implementation of braking instructions will greatly protect the personal safety of the driver and passengers.

Permanent magnet synchronous motors (PMSM) are very suitable as drive motors of EVs, due to their high efficiency, high-power density, high reliability, and wide speed range [5]. While model predictive control (MPC) for PMSM can achieve satisfactory dynamic performance, it comes with a relatively high calculation burden even with pre-selection process of the candidate voltage vectors [6], [7], and tuning its weighting factors is difficult [8], [9]. Conventional deadbeat predictive current control (DPCC) has received widespread attention due to its low calculation burden and comparable performance to MPC [10]. However, conventional DPCC relies on an accurate motor model for calculating the voltage command, making its performance highly sensitive to parameter accuracy [11]. To address performance degradation caused by parameter mismatch, various solutions have been proposed.

Common solutions include parameter identification and disturbance observer techniques. Identification techniques involve identifying machine parameters, such as stator resistance, stator inductance, etc., either prior to or during motor operation, and then incorporating these identified machine parameters into calculations. For instance, in [12], authors use the Kalman Filter to identify the machine parameters. Improved model reference adaptive systems for online parameter identification are proposed in [13] and [14]. Differ from identification techniques, disturbance observer techniques aim to generate a compensating term to suppress steady-state errors without identifying the exact parameter mismatch. Many different types of observers have been investigated to handle the disturbance caused by parameter or model uncertainties, such as various sliding mode observers (conventional [15], second-order [16], high-order [17], and composite [18] SMOs), traditional and improved stator current and disturbance observers [19], [20], linear disturbance

Manuscript received Month xx, 2xxx; revised Month xx, xxxx; accepted Month x, xxxx. This work was supported by "the Fundamental Research Funds for the Central Universities", Sichuan University (Grant Number: YJ202453). *(Corresponding author: Dong Wang, Kaiyuan Lu).*

Chao Zhang is with the School of Electrical Engineering, Beijing Jiaotong University, 100044 Beijing, China (e-mail: 18117026@bjtu.edu.cn).

Dong Wang is with the College of Electrical Engineering, Sichuan University, 610065 Sichuan, China (e-mail: dw@scu.edu.cn).

Kaiyuan Lu is with the Department of Energy Technology, Aalborg University, 9220 Aalborg, Denmark (e-mail: klu@energy.aau.dk).

Mentions of supplemental materials and animal/human rights statements can be included here.

Color versions of one or more of the figures in this article are available online at http://ieeexplore.ieee.org

observer [21], Luenberger observer [22], and extended state observer [23]. Additionally, numerical integration term [24], integral controller [25], and voltage compensation term based on the error of current prediction [11] can be used for compensating current steady-state errors. Besides the above model-based methods, model-free DPCC (MF-DPCC) combines all known and unknown parts of the machine model into one unknown disturbance and forms a first-order ultra-local model to represent the machine model [26], [27]. The unknown disturbance and gain of the system input can be determined by adopting an ESO [26] or calculated based on current variations [27].

The above methods can well enhance the parameter robustness of conventional DPCC to ensure zero steady-state error. However, most of them did not focus on the impact of parameter mismatch on system's transient performance. According to the experiment results provided by the above literatures, it is found that 30~50 sampling/switching periods are generally required for parameter identification [12], [13]. For electrical machines with small inductance variation due to magnetic saturation, the estimation error caused by load changes would be small, resulting in little impact on the system's transient performance. While for electrical machines with relatively large inductance variation due to magnetic saturation, additional time is required for the parameter identification method to converge to the new value, which indicates that the transient of the current step response would be long and further research effort is needed.

Regarding observer-based DPCC methods, the transients of the current step response take 60-100 sampling/switching periods in most of the methods [15], [16], [18], [21]. Some methods offer improved transient performance, requiring only 15-20 sampling/switching periods for the current step response [17], [22], [23]. Among all the above methods, the method with closed-form error compensation (CEC) [11], which calculates a compensated term based on current prediction error, provides the most promising transient performance, needing only 12 sampling/switching periods. However, the performance of the DPCC-CEC method proposed in [11] degrades fast as the parameter mismatch increases. Experiments in this study show that when the inductance deviation exceeds ±30%, the DPCC-CEC method results in significant oscillation and prolonged settling time.

Based on the above analysis, while the impact of parameter mismatch on steady-state performance has been effectively mitigated, the existing literature does not adequately address its impact on dynamic performance. This paper proposes an adaptive linear predictive deadbeat control (ALPDC) method that can greatly enhance the dynamic tracking performance against parameter uncertainty for surface-mounted PMSM (SPMSM) drives. The proposed ALPDC method introduces two sampling/switching periods to determine the actual machine response characteristic by measuring the current response of a test voltage. Thereafter, the final required voltage command, which can bring the current to its new reference value during the third sampling period, is determined by utilizing the actual machine response characteristic. This method is simple to implement and prevents current overshoots caused by machine inductance mismatch during transients.

This paper focuses on transient performance enhancement under parameter mismatch conditions. The steady-state control is realized by the advanced DPCC techniques such as the DPCC-CEC method proposed in [11], whose steady-state performance is satisfactory but its transient performance should be enhanced to handle the parameter mismatch to a larger extent. As demonstrated by various experimental results in Section IV, the proposed solution significantly enhances the transient performance compared to using DPCC-CEC alone under conditions of large parameter mismatch.

The rest of this paper is organized as follows: The DPCC-CEC method proposed in [11] is reviewed in section II, representing a benchmark advanced DPCC technique. Section III introduces the principle of the proposed ALPDC. Experimental results, including a comparison with and without ALPDC-incorporated DPCC-CEC, are given in section IV for validation. To illustrate the compatibility of the proposed method, the ALPDC is also incorporated into another advanced DPCC technique that utilizes a disturbance observer [19]. Extended experimental results, both with and without ALPDC-incorporated DPCC with a disturbance observer, are given in this section. Section V concludes this paper.

II. Deadbeat Predictive Current Control With Closed-Form Error Compensation

A. SPMSM model in the d-q axis

The mathematical model of the SPMSM in the d-q axis can be expressed as

$$u_{\mathrm{dq}} = R_{\mathrm{s}} i_{\mathrm{dq}} + j\omega_{\mathrm{e}} L_{\mathrm{s}} i_{\mathrm{dq}} + j\omega_{\mathrm{e}} \psi_{\mathrm{f}} + L_{\mathrm{s}} \frac{di_{\mathrm{dq}}}{dt} \tag{1}$$

where $f_{\mathrm{dq}} = f_{\mathrm{d}} + jf_{\mathrm{q}}$ and f represents either the current or voltage; R_{s} is the stator resistance; L_{s} is the stator inductance and $L_{\mathrm{s}} = L_{\mathrm{d}} = L_{\mathrm{q}}$ for SPMSM; Ψ_{f} is the permanent magnet (PM) flux linkage; ω_{e} is the electrical angular velocity.

B. Principle of DPCC-CEC

In discrete-time control theory, deadbeat control aims to determine the system input that can bring the output to its reference in the fewest possible steps. Traditional DPCC aims to calculate the voltage command based on the current command and machine parameters to achieve current tracking within a single control cycle.

However, due to the inevitable digital implementation delay, the voltage calculated in the current switching period can only influence the current change in the subsequent switching period. Therefore, it is necessary to predict the current at the end of the current switching period. The predictive current equation can be obtained by discretizing (1) using first-order forward Euler method.

$$\hat{i}_{\mathrm{dq}}(k+1) = (1 - \frac{R_{\mathrm{s}} T_{\mathrm{s}}}{L_{\mathrm{s}}} - j\omega_{\mathrm{e}} T_{\mathrm{s}}) i_{\mathrm{dq}}(k) + \frac{T_{\mathrm{s}}}{L_{\mathrm{s}}} [u_{\mathrm{dq}}(k) - j\omega_{\mathrm{e}} \psi_{\mathrm{f}}] \tag{2}$$

where the hat symbol represents the predictive value; T_{s} is the switching period.

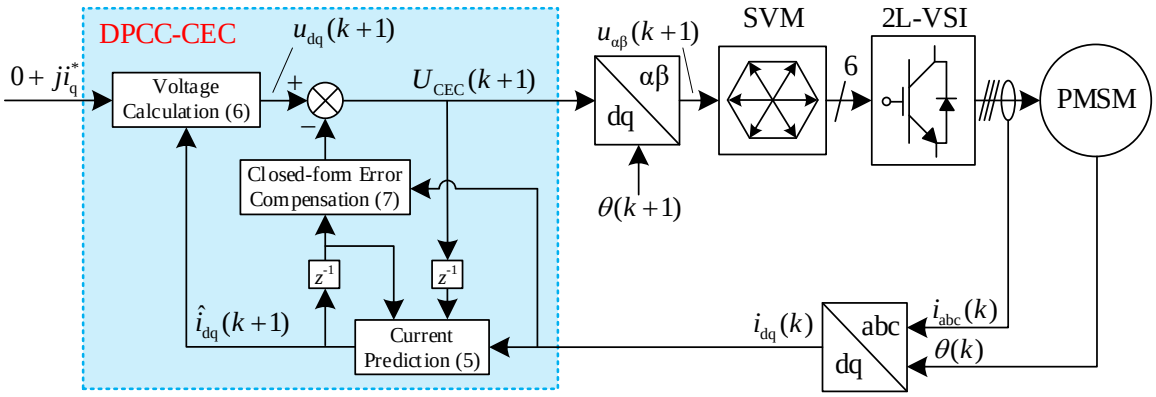

Fig. 1. Block diagram of DPCC-CEC proposed in [11].

When the system parameters are accurate, the stator current can track the current command within a single control cycle according to the fundamental principle of DPCC. The stator current at the (k+2)th instant would be equal to the current command. Therefore, the voltage applied at the (k+1)th instant can be expressed as

$$u_{dq}(k+1)=\frac{L_s}{T_s}[i_{dq}^*(k+2)-(1-\frac{R_sT_s}{L_s}-j\omega_eT_s)\hat{i}_{dq}(k+1)] +j\omega_e\psi_f \quad (3)$$

where i_{dq}^* is the stator current command vector and $i_{dq}^*=0+ji_q^*$ when the motor is controlled by $i_d^*=0$.

According to (3), the calculated voltage is highly dependent on the motor parameters, and inaccurate parameter values can lead to current steady-state errors. Therefore, [11] proposes a simple voltage compensation term linked to the difference between predicted and measured currents in the current period. The calculated voltage after compensation, which is output in the next control period, can be expressed as

$$U_{CEC}(k+1)=u_{dq}(k+1)-\underbrace{\frac{L_s}{T_s}(2-j\omega_eT_s)[i_{dq}(k)-\hat{i}_{dq}(k)]}_{\text{compensation term}}. \quad (4)$$

Considering that external disturbances and sample noise can affect the stability of the practical system, as presented in reference [11], the equations (2) - (4) have been improved through the introduction of noise suppression schemes. The improved equations are expressed as

$$\hat{i}_{dq}(k+1)=(1-\frac{R_sT_s}{L_s}-j\omega_eT_s)\hat{i}_{dq}(k) +\frac{T_s}{L_s}[U_{CEC}(k)-j\omega_e\psi_f]+l_1[i_{dq}(k)-\hat{i}_{dq}(k)] \quad (5)$$

$$u_{dq}(k+1)=\frac{L_s}{T_s}\left\{\begin{array}{l}i_{dq}^*(k+2)+l_2[i_{dq}^*(k+1)-\hat{i}_{dq}(k+1)]\\-(1-\frac{R_sT_s}{L_s}-j\omega_eT_s)i_{dq}^*(k+1)\end{array}\right\} +j\omega_e\psi_f \quad (6)$$

$$U_{CEC}(k+1)=u_{dq}(k+1)-\underbrace{\frac{L_s}{T_s}l_3[i_{dq}(k)-\hat{i}_{dq}(k)]}_{\text{compensation term}} \quad (7)$$

where l_1, l_2, and l_3 are constant feedback gains and their selection principle is the same as that used in [11].

The structure of the DPCC-CEC, selected as a benchmark advanced DPCC technique, is illustrated in Fig. 1 in accordance with (5) - (7).

III. Adaptive Linear Predictive Deadbeat Control

It is well known that the performance of the conventional DPCC heavily depends on motor parameter accuracy. Although the DPCC-CEC method proposed in [11] can well mitigate the steady-state error caused by the parameter mismatch, it offers limited improvement in transient performance. For instance, DPCC-CEC requires only about 6 switching periods to respond to a step change without noticeable oscillation when the inductance mismatch range is approximately ±10%, as demonstrated by the experimental results in both [11] and this paper. However, the settling time and the transient oscillations become more pronounced as the mismatch range increases. To enhance the transient performance of DPCC-CEC, a new dynamic tracking method named ALPDC is proposed in this paper.

A. Basic principle

For an SPMSM, where $i_d = 0$ is often chosen, (1) may be discretized by using the first-order forward Euler method as

$$u_q(k)=R_si_q(k)+\psi_f\omega_e(k)+\frac{L_s}{T_s}[i_q(k+1)-i_q(k)]. \quad (8)$$

In steady state, i.e., $i_q(k+1) = i_q(k)$, the third term on the right side of (8) will disappear. It is evident that the first term on the right side of (8) is the voltage drop on the resistance, and the second term is the back EMF. The sum of these two terms is defined as the steady-state voltage component U_{st}. The third term is defined as the dynamic voltage component U_{dy}. Equation (8) may then be rearranged as

$$\left\{\begin{array}{l}u_q=U_{st}+U_{dy}\\U_{st}=k_1i_q+k_2n\\U_{dy}=k_3\Delta i_q\end{array}\right. \quad (9)$$

$$\left\{\begin{array}{l}k_1=R_s\\k_2=p_n\psi_f\pi/30\\k_3=L_s/T_s\end{array}\right. \quad (10)$$

where n is the motor mechanical speed in r/min; p_n is the

number of pole pairs; k_1, k_2, k_3 are the coefficients defined by the machine parameters. It should be noted that k_1, k_2, k_3 are not gain factors that require tuning.

When the current command is suddenly changed, an appropriate dynamic voltage component U_{dy} should be determined. The ideal U_{dy} should bring the current to its new reference value within one switching period. However, achieving an ideal U_{dy} is challenging due to the difficulty in ensuring that the coefficient k_3 can consistently obtain an accurate value under varying transient conditions. The main idea of the proposed ALPDC method is to insert two test voltage commands before calculating the final required voltage command to bring the current to its new reference value. This procedure is explained in detail in Fig. 2.

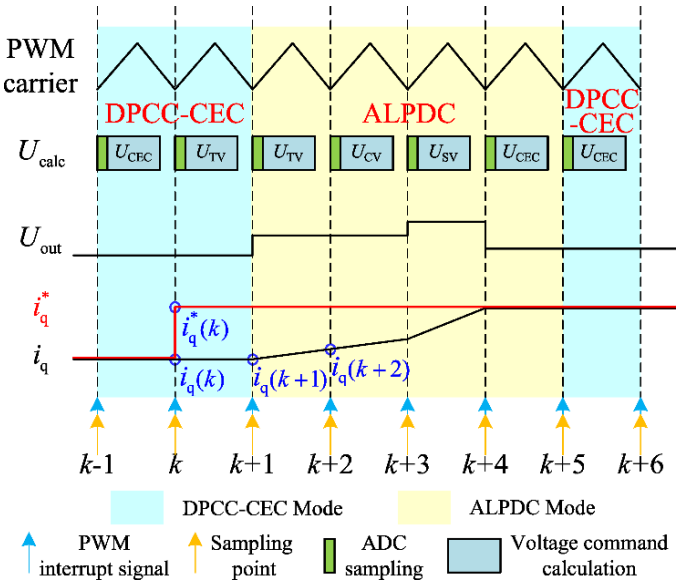

Fig. 2. Timing diagram showing the ALPDC principle.

In Fig. 2, the voltage command is calculated upon detecting a change in the current reference. However, this command will be physically generated by the inverter in the next switching period due to digital implementation delay. The calculated and output voltage commands are defined as U_{calc} and U_{out} in Fig. 2, respectively. As may be observed from Fig. 2,

1) at t = k-1, the controller is in its steady state and the voltage command (U_{CEC}) is generated by the DPCC-CEC controller.
2) at t = k, a new current command is received, and the test voltage command (U_{TV}) is calculated. It should be noted that, due to the digital implementation delay, the voltage command calculated in this switching period [k, k+1] will be generated in the next switching period, i.e., the new U_{TV} will cause the current to change from t = k+1. This test voltage is determined to adjust the current to a specific percentage of the variation in the current command. Please refer to the determination principle of factor k_{dy} in section III.C.
3) at t = k+1, there is no useful feedback information available yet, and the voltage for the next period [k+2, k+3] needs to be determined in this switching period. The same test voltage is then repeated. It is therefore expected that the current variation during [k+2, k+3] will be the same as that during [k+1, k+2] when considering SPMSM with small inductance variation. Please refer to the discussion related to (11).
4) at t = k+2, now the current variation due to the first test voltage can be obtained and it can be used to find the actual current change rate. Since the same current variation is expected for the period [k+2, k+3] as mentioned in the above step, the current at the end of this period can be easily predicted without relying on machine equations or parameters. By using the predicted current at t = k+3 and knowing the difference between the predicted current at t = k+3 and the reference current, along with the measured correct current change rate from the first test voltage, a correction voltage U_{CV} can be calculated in this period and generated in the next period. Please refer to (14) regarding the calculation of U_{CV}.
5) at t = k+3, since it is expected that the current at the end of this switching period will be the reference current, the new steady-state voltage command U_{SV} to be available at the beginning of t = k+4 will be calculated.
6) at t = k+4, the current reaches the reference current and the controller will be switched back to DPCC-CEC.

The proposed ALPDC exhibits strong robustness to parameter mismatch by simply adding test and measurement voltage periods.

B. Current prediction

The calculation of the voltage command needs the current information, as specified in (8). However, due to digital implementation delay, the voltage calculated in the current switching period can only affect the current change in the next switching period. Therefore, it is essential to know the current value at the end of the current switching period (beginning of the next switching period) for prediction purposes. This is why in the proposed method, the same test voltage is applied for two consecutive switching periods. By selecting a proper value of the test voltage, whose selecting principle is described in the following part, a linear current response can be expected. This allows for a simplified current prediction at the end of the second test voltage period (beginning of the correction voltage period at t = k+3) that does not rely on motor parameters. In fact, it simply utilizes the same current variation obtained during the first test voltage period, i.e.,

$$\hat{i}_q(k+3) - i_q(k+2) = i_q(k+2) - i_q(k+1). \qquad (11)$$

During transient operation, considering that the current change in each period during [k+1, k+3] is about 25% of the command change, the variation of the actual current changes between two adjacent switching periods is relatively small, especially for SPMSM. The measured difference between full-load and no-load inductance is only 2% for the test SPMSM. Therefore, (11) can reliably predict the actual current at t = k+3 based on the currents measured at t = k+1 and t = k+2. In

steady state, (11) does not need to be activated, since the DPCC-CEC method proposed by [11] has effectively addressed the steady-state current prediction problem.

C. Voltage command calculation

As referenced in (9), the dynamic voltage component required to bring the current to its new reference value can be calculated as follows

$$\begin{cases} U_{\mathrm{dy}} = k_3[i_{\mathrm{q}}^*(k) - i_{\mathrm{q}}(k)] \\ U_{\mathrm{TV}} = k_{\mathrm{dy}}U_{\mathrm{dy}} + U_{\mathrm{st\_old}} \end{cases} \tag{12}$$

where $U_{\mathrm{st\_old}}$ is the steady-state voltage command applied in the (k)th control cycle; k_{dy} is the scaling factor.

The value of k_{dy} is determined by the following principle: it is expected that there is no overshoot during the current step response, i.e., the actual current at time instant k+3 in Fig. 2 does not exceed the current command. For the ideal condition where k_3 is accurate (i.e. no parameter mismatch), if k_{dy} is chosen to be 0.5, the current will reach its command value exactly after the two test voltage periods. However, if there is a parameter mismatch causing k_3 used in the controller is 1.5 times of the actual value, to make sure that the current will not exceed its command after two test voltage periods, the test voltage should be limited to 2/3 (1/1.5 = 2/3), which means that the upper limit of k_{dy} should not exceed 1/3 (i.e. half of 2/3).

Moreover, it should be noted that the above determination principle (i.e. no overshoot during the current step response) also ensures that the required voltages used in the proposed method will not exceed the available voltage (e.g. the required duty cycle will not exceed 1 during the SVM calculation). This means that there is no unexpected nonlinearity caused by voltage saturation. Assuming that the voltage margin is just sufficient for the conventional deadbeat control to achieve a current step change from no-load to rated-load condition when the motor operates at its rated speed, a large parameter mismatch would mean there is not enough voltage available to meet the requirement of the conventional deadbeat control. Taking the above condition where k_3 used in the controller is 1.5 times the actual value as an example, the voltage required by the conventional deadbeat control algorithm will be 1.5 times the available voltage. This will cause duty cycle saturation problem during SVM calculation, which will result in voltage error and system nonlinearity. Thus, the test voltage applied to the two test periods during [k+1, k+3] should be limited to 2/3, which means that the upper limit of k_{dy} should not exceed 1/3. This is exactly the same conclusion as the one obtained by the above determination principle.

Considering that the dc-link voltage may reduce during step load change condition, k_{dy} is selected to be 0.25 in this paper.

At the start of the second test voltage period, the actual current variation can be measured and the parameter k_3 can be corrected as

$$\hat{k}_3 = \frac{k_{\mathrm{dy}}U_{\mathrm{dy}}}{i_{\mathrm{q}}(k+2) - i_{\mathrm{q}}(k+1)} \tag{13}$$

where $\hat{k}_3$ is the corrected value of k_3.

Since (13) is only used during the [k+2, k+3] period, the issue of $\hat{k}_3$ being too large caused by the denominator being equal to zero is safely avoided. After knowing the corrected k_3 (i.e. $\hat{k}_3$) and the predicted current at t = k+3, the correction voltage for the final switching period to bring the current to its reference value can be determined as

$$U_{\mathrm{CV}} = \hat{k}_3[i_{\mathrm{q}}^*(k) - \hat{i}_{\mathrm{q}}(k+3)] + U_{\mathrm{st\_old}}. \tag{14}$$

In (14), the steady-state voltage offset is simply the previous value $U_{\mathrm{st\_old}}$ at t = k. This is because U_{st} during interval [k, k+3] can be assumed to be constant and is equal to the voltage command at time t = k ($U_{\mathrm{st\_old}}$) due to relatively very small resistive voltage change compared to the actual voltage command in fast current change dynamics. For example, according to the experimental results shown in Fig. 8, the resistive voltage change is only about (32.8722-25.6893)/150.53 ≈ 4.7% of the calculated voltage command at time k+3.

The current will complete current tracking during the (k+3)th switching period. Following that, the DPCC-CEC controller takes over the control for the continued steady-state operation. Due to the digital implementation delay, a switching period needs to be added to facilitate a smooth transition from ALPDC to DPCC-CEC. This switching period aims to maintain the current at an approximately constant level, and the calculation equation of the new steady state voltage command U_{SV} is expressed as

$$U_{\mathrm{SV}} = k_1 i_{\mathrm{q}}^* + k_2 n. \tag{15}$$

Although the U_{SV} may deviate from the expected value due to inaccuracies in k_1 and k_2, this deviation is relatively small compared to the voltage across the inductor in dynamics. As a result, even with inaccuracies in k_1 and k_2, the U_{SV} will not cause significant changes in the current. Any small steady-state error in the current, caused by the inaccuracies in k_1 and k_2, will be mitigated by the compensation term introduced in the DPCC-CEC. This has been well demonstrated in [11].

D. Implementation of ALPDC

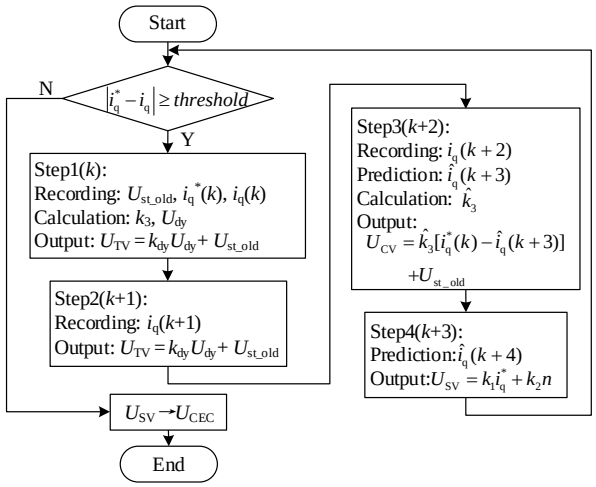

Fig. 3. The flow chart of ALPDC structure.

The ALPDC controller aims to calculate the q-axis voltage

command. The flow chart for determining the transient voltage commands is summarized in Fig. 3.

Regarding the current error "threshold" involved in Fig. 3, its value is chosen to be about 3 times the peak value of the current ripple observed at the steady state to ensure that the proposed method will not be mis-triggered by the current ripples while it can respond to notable changes of the current command. In this paper, the threshold value is chosen to be 1A, since the peak value of the current ripple at steady state is about 0.3A as can be observed later in Fig. 6.

IV. Experimental Results

To demonstrate the effectiveness of the proposed method, experiments using a SPMSM drive system were conducted. The main parameters for the SPMSM are given in Table I. The experimental platform, as depicted in Fig. 4, comprises a dSPACE MicroLabBox (DS1202), a test motor, a load motor, an inverter, and a PC. The switching and sampling frequencies are set at 5kHz. The test motor operates under current control, while the load motor is subjected to speed control.

TABLE I
PARAMETERS OF THE SPMSM

Symbol	Quantity	Value
R_s	Stator resistance	0.75 Ω
L_s	Stator inductance	6.4 mH
Ψ_f	PM flux linkage	0.1213 Wb
p_n	Pole pairs	4
n	Maximum speed	4500 r/min
I_{rated}	Rated current	8 A
P_{rated}	Rated power	2.7 kW
f_s	Switching frequency	5 kHz

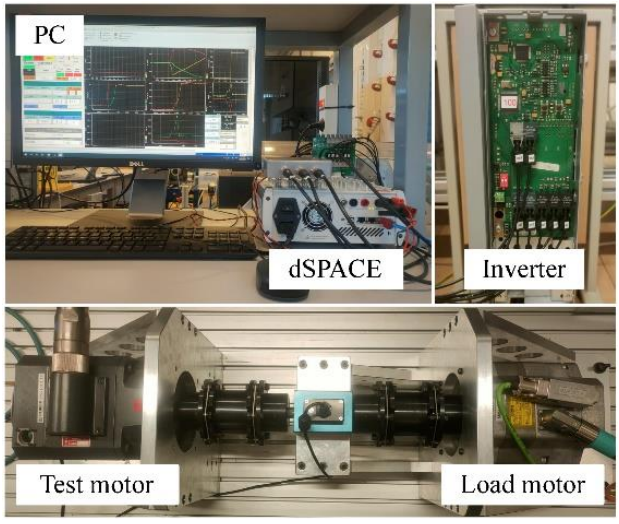

Fig. 4. Experimental platform of SPMSM drive system.

The following parts of this section are: Part A demonstrates the performance of the proposed method at different speeds. Part B examines the performance under parameter mismatch, including a comparison of DPCC-CEC without and with the introduction of ALPDC. In part C, the proposed ALPDC structure is further tested with a DPCC controller that employs a disturbance observer (referred to as DPCC-DO). In this paper, the proposed stator current and disturbance observer in [19] is used as an example. All the comparison results without and with ALPDC indicate that the proposed ALPDC can enhance the transient performance and exhibit good compatibility.

For clarity, the method of ALPDC combined with DPCC-CEC is referred to as ALPDC-CEC in the following parts. Similarly, the method of ALPDC combined with DPCC-DO is referred to as ALPDC-DO.

A. Performance of ALPDC-CEC under different speeds

To demonstrate that the proposed ALPDC can track the current command within three control cycles, rated current step commands are executed at 500 r/min and 4500 r/min (rated speed), respectively. The corresponding results are shown in Fig. 5 and Fig. 6. According to the previous analysis, values for k_{dy} and the current error threshold are selected to be 0.25 and 1A, respectively.

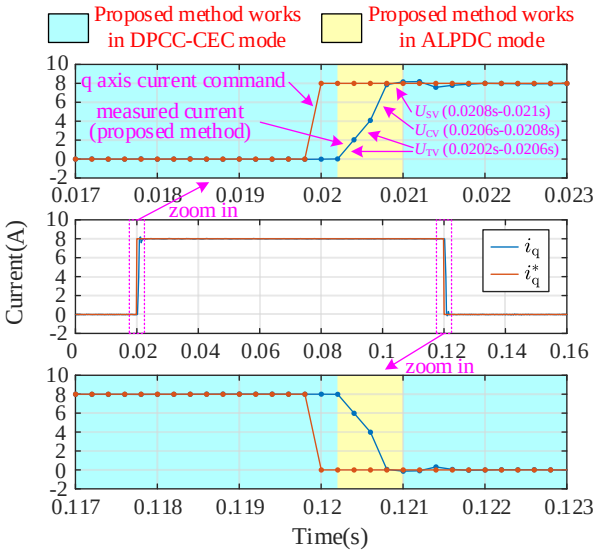

Fig. 5. The q-axis current response at 500 r/min with current command stepping from zero to rated current at 0.02s and from rated current to zero at 0.12s.

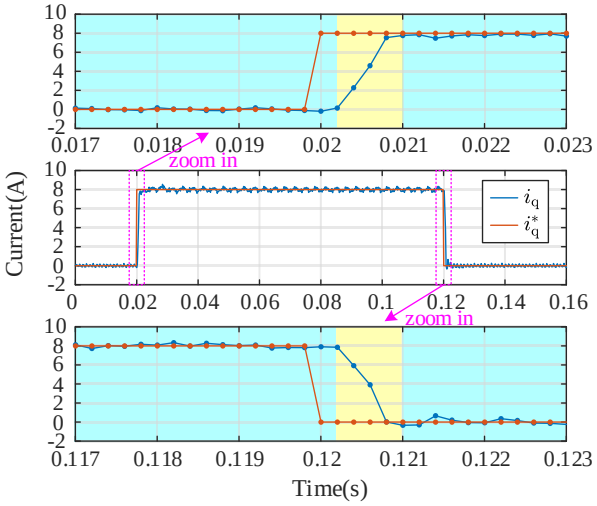

Fig. 6. Current response at 4500 r/min with current command stepping from zero to rated current at 0.02s and stepping from rated current to zero at 0.12s.

Fig. 7 and Fig. 8 show the corresponding phase current and the calculated q-axis voltage command during the transients of current step response shown in Fig. 5, respectively.

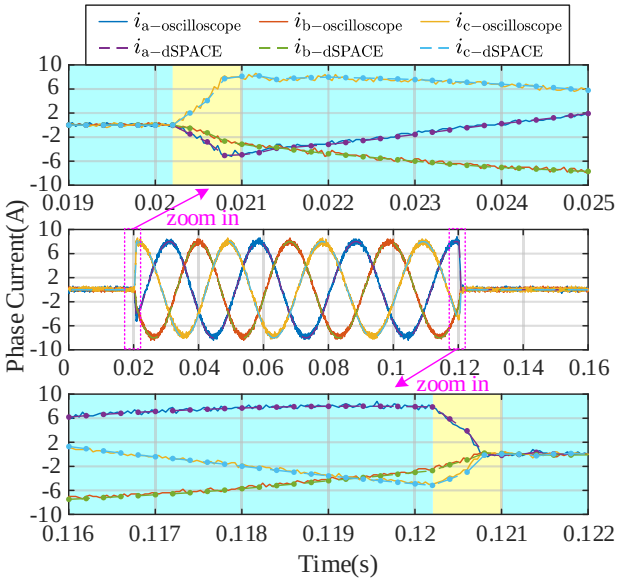

Fig. 7. Phase current response at 500 r/min with current command stepping from zero to rated current at 0.02s and from rated current to zero at 0.12s. (The data of the solid and dotted waveforms are obtained from the oscilloscope and dSPACE, respectively)

The three-phase motor current is shown in Fig. 7. It can be observed that the actual currents captured by the oscilloscope appear noisier, as the current ripples caused by switching actions are captured. While the dSPACE system samples the data once per switching period, effectively reducing the switching ripples through the sampling process. However, the currents measured by dSPACE are still very good representations of the actual currents, as shown in the comparison in Fig. 6. Therefore, it is feasible to use the data obtained from dSPACE to verify the accuracy and effectiveness of the proposed ALPDC method. Moreover, it can be observed again from the three-phase motor currents that there are no spikes during the step response transients, and the transition between DPCC-CEC method and proposed method is very smooth.

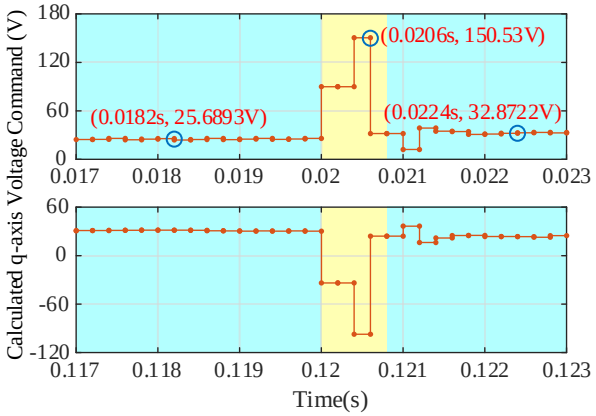

Fig. 8. The calculated q-axis voltage command at 500 r/min. (a) Current command steps from zero to rated current at 0.02s. (b) Current command steps from rated current to zero at 0.12s.

The results in Fig. 8 indicate that the current command steps from zero to its rated value at t = 0.02s, and the test voltage is calculated at the same time. It will affect the current change in the next two control cycles (0.0202s~0.0206s). Linear current changes during these two control periods can be observed in Fig. 5. Meanwhile, correction voltage U_{CV} is calculated in the period from 0.0204s to 0.0206s, affecting the current in the next control cycle. The current reaches the new command current at 0.0208s. Following this, the DPCC-CEC controller takes over the control for continued steady-state operation. Similar performance can also be observed when operating at the rated speed of 4500 r/min, as shown in Fig. 6.

B. The performance comparison between ALPDC-CEC and DPCC-CEC with parameters mismatch

The influence of motor parameter mismatch on current response is analyzed in this section, for the conventional DPCC-CEC and the proposed ALPDC-CEC. Given that these two methods exhibit similar performance at different speeds, the following experiments are carried out at 500 r/min as an example. Fig. 9 shows the current response with inductance mismatch for DPCC-CEC and ALPDC-CEC respectively.

It may be observed from Fig. 9 (a) that the performance of DPCC-CEC is closely linked to the range of inductance mismatch. When motor parameters are accurate, the actual current tracks the command in one control cycle, aligning with the ideal DPCC performance. Due to its modest transient parameter robustness, DPCC-CEC exhibits minimal disruption to the settling time and transient oscillation, with a ±15% inductance mismatch range (as seen in the green and purple curves in Fig. 9 (a)). For instance, the settling time is about 6 switching periods, and the current transient oscillation is not obvious, akin to the experimental result reported in [11]. However, as the inductance mismatch range continues to increase, the transient performance of DPCC-CEC is severely compromised. For instance, with a ±30% inductance mismatch, as depicted by the dark red and yellow curves in Fig. 9 (a), the settling time increases to several dozen switching periods, and the maximum overshoot during the transient reaches 25.5% and 29.3%, respectively.

Fig. 9 (b) shows the current response of the proposed ALPDC-CEC under inductance mismatch. According to (10) and (12), the test voltage U_{TV}, determined by k_3, varies for different inductance values, leading to different slopes during the first two switching periods (0.0202s ~ 0.0206s) when the test voltage commands dominate the transient performance. However, the inaccurate k_3 will be corrected using (13) based on the actual current response between 0.0202s and 0.0204s before calculating the correction voltage command U_{CV}. This allows the correct correction voltage to be generated, bringing the current to its desired reference value at 0.0208s. Because the DPCC-CEC method can well reduce the current steady-state error caused by inaccurate resistance and flux linkage, the current quickly reaches a steady state and maintains good steady-state performance. Compared to Fig. 9 (a) of the DPCC-CEC method, under the same working conditions (i.e., ±30% mismatch, as seen in the green and purple curves in Fig. 9 (b)), the proposed method exhibits significantly better

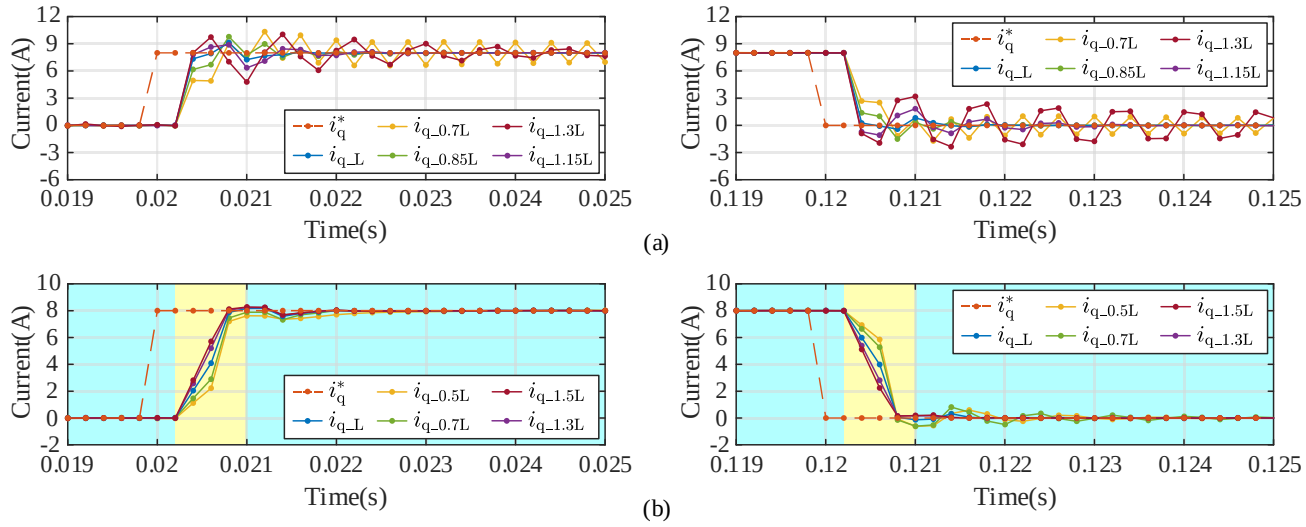

Fig. 9. Current responses of two control methods with stator inductance mismatch. (a) DPCC-CEC. (b) ALPDC-CEC. (Current command steps from zero to rated current at 0.02s and from rated current to zero at 0.12s.)

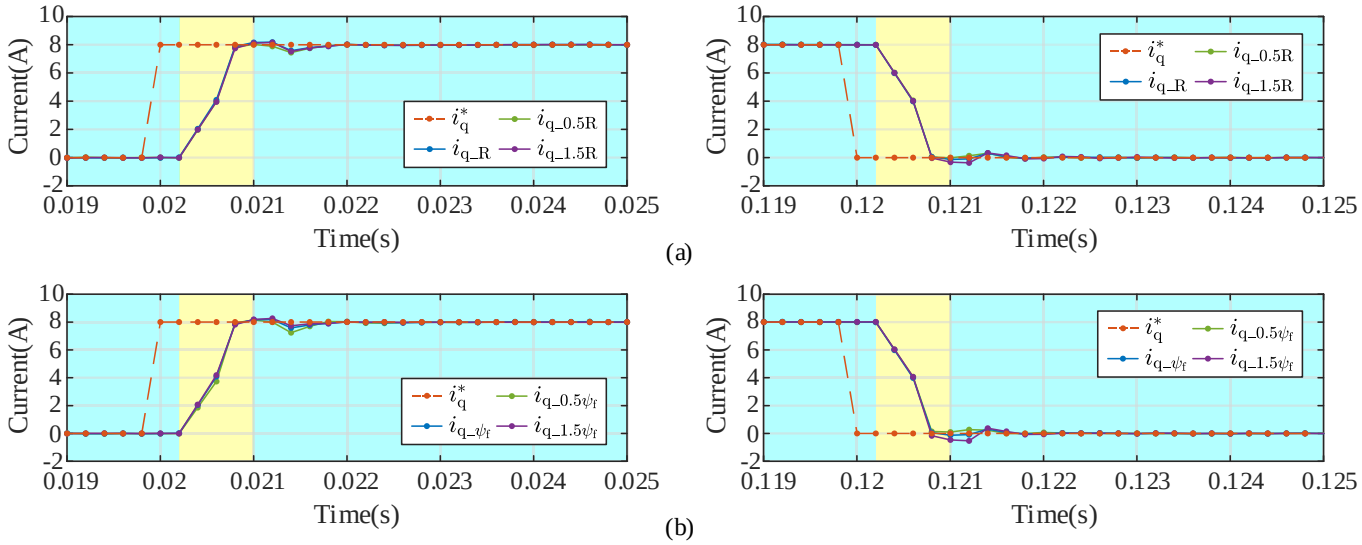

Fig. 10. Current responses of ALPDC-CEC with stator resistance and flux linkage mismatch respectively. (a) Resistance mismatch. (b) Flux linkage mismatch. (Current command steps from zero to rated current at 0.02s and from rated current to zero at 0.12s)

dynamic responses with no overshoot. Furthermore, even when the inductance mismatch range increases to ±50% (as depicted by the yellow and dark red curves in Fig. 9 (b)), ALPDC-CEC can still achieve good dynamic and steady-state performance.

The subplots (a) and (b) of Fig. 10 show the current transient performance of ALPDC-CEC with resistance and flux linkage mismatch, respectively. According to (9) and (10), resistance and flux linkage alter the steady-state voltage component by affecting k_1 and k_2, respectively. Similarly, inductance affects dynamic voltage component by influencing k_3. In Fig. 10, the change in current during the dynamic process remains consistent when stator resistance and flux linkage are set at 0.5, 1, and 1.5 times the actual values, respectively. This is because the dynamic voltage component commands do not rely on resistance and flux linkage in ALPDC. The resistance and flux linkage mainly affect the steady-state current value, which is effectively compensated by the CEC term, ensuring no steady-state tracking error.

Based on the above analysis, the proposed ALPDC structure not only maintains the strong steady-state parameter robustness of DPCC-CEC but also greatly improves the transient parameter robustness.

C. Extended application of ALPDC structure

According to the introduction in section I, the disturbance observer technique is commonly used to improve the parameter robustness of conventional DPCC by estimating the voltage error caused by the parameter mismatch. Although this method could effectively compensate for the voltage error, it is limited by the observation speed of the disturbance observer (DO) and cannot achieve the nearly ideal deadbeat predictive current control. Moreover, the transient performance relies heavily on the accuracy of the inductance value. Therefore, the method using DO faces the same transient performance problem as the DPCC-CEC method described above.

To address the aforementioned problem, the ALPDC

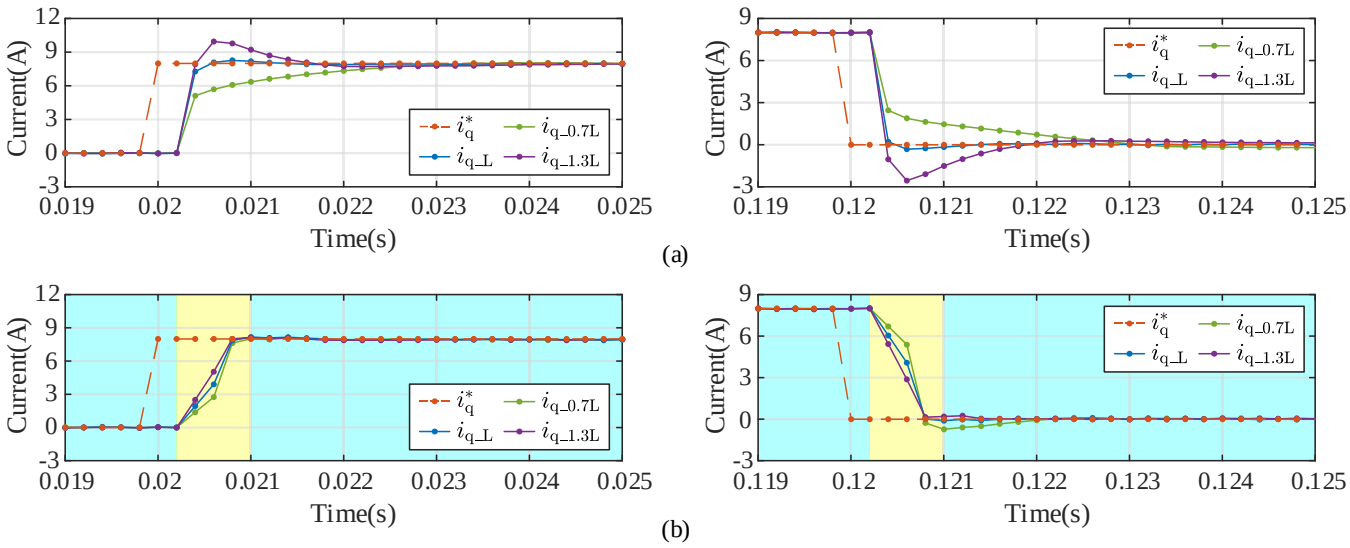

Fig. 11. Current responses of two control methods with stator inductance mismatch. (a) DPCC-DO. (b) ALPDC-DO. (Current command steps from zero to rated current at 0.02s and from rated current to zero at 0.12s)

structure proposed in this paper is extended to the DPCC method with a disturbance observer (referred to as DPCC-DO). The stator current and disturbance observer proposed in [19] is used as an example. In the subsequent content, the DPCC-DO method proposed in [19] is used as a test platform of the extended application to demonstrate that the proposed ALPDC method can further improve transient performance when incorporated with the DPCC-DO. The comparative experimental results without and with ALPDC structure are shown in Fig. 11.

In Fig. 11 (a), it can be seen that when a step command is applied and there is an inductance mismatch of ±30%, the voltage command obtained through the conventional DPCC-DO method is not accurate and results in large current errors. The voltage error between the incorrect and ideally calculated command hinders the accurate tracking of the actual current to the command within the desired time. Although the DO can well compensate for the voltage error, when the inductance mismatch is ±30%, the process requires at least about 7~10 control cycles, and the maximum current deviation relative to the command is about 2~3 A during this process. This experimental result indicates that the transient performance is severely compromised when the inductance mismatch is about ±30%.

However, with the introduction of the ALPDC structure, the significantly compromised transient performance has been greatly improved. Within the first three switching periods after a step command, the ALPDC structure ensures that the actual current reaches the command value. At the same time, the estimated inductance value ($\hat{L}_s = \hat{k}_3 T_s$) is updated in DO to ensure that the DO provides the correct observation result, allowing for a smooth transition from ALPDC to DPCC-DO. For instance, as shown in Fig. 11 (b), even with a deviation of ±30% in the inductance value used in the controller, the actual current can reach the command value at approximately 0.0208s, smoothly transitioning to DPCC-DO mode without noticeable dynamic oscillation and steady-state error.

The above experimental results have clearly shown the superior performances and good compatibility of the proposed ALPTC structure for current transient regulation compared to the conventional methods, such as DPCC-CEC and DPCC-DO.

V. Conclusion

A method named ALPDC has been proposed in this paper to enhance the transient performance of SPMSM, making it robust against parameter uncertainty. Experimental evidence has shown that the performance of the DPCC-CEC method, as proposed in [11], significantly deteriorates with an inductance mismatch range of ±30%. The proposed ALPDC method effectively solves this problem by introducing test, measurement, and correction voltage periods. It is a simple and easily implementable solution. The dynamic current tracking can be accomplished in three switching periods, and its performance remains robust to parameter mismatch, overcoming the main challenges faced by DPCC-CEC. Despite the addition of two extra switching cycles, the dynamic performance of ALPDC outperforms the existing advanced methods using “Closed-form Error Compensation (CEC)” term [11] and “Stator Current and Disturbance Observer” [19]. These experimental results further validate the good compatibility of the proposed ALPDC structure, showcasing its adaptability to different DPCC structures. It should be pointed out that the proposed method has mainly been verified on SPMSM drives. The performance and suitability of the proposed method under other operation conditions, as well as for other machine types such as interior PMSM, will be further studied in future work.

References

[1] A. M. Dizqah, B. Lenzo, A. Sorniotti, P. Gruber, S. Fallah and J. De Smet, “A Fast and Parametric Torque Distribution Strategy for Four-Wheel-Drive Energy-Efficient Electric Vehicles,” *IEEE Trans. Ind. Electron.*, vol. 63, no. 7, pp. 4367-4376, July 2016.

[2] S. Bolognani, R. Petrella, A. Prearo and L. Sgarbossa, “Automatic

Tracking of MTPA Trajectory in IPM Motor Drives Based on AC Current Injection," *IEEE Trans. Ind. Appl.*, vol. 47, no. 1, pp. 105-114, Jan.-Feb. 2011.

[3] S. Kim, Y. -D. Yoon, S. -K. Sul and K. Ide, "Maximum Torque per Ampere (MTPA) Control of an IPM Machine Based on Signal Injection Considering Inductance Saturation," *IEEE Trans. Power Electron.*, vol. 28, no. 1, pp. 488-497, Jan. 2013.

[4] I. Spina and A. Cervone, "Energy saving in Battery Electric Vehicles equipped with Induction Machines and Modular Multilevel Converters," *in IEEE Int. Conf. Compat., Power Electron. Power Eng., (CPE-POWERENG)*, Florence, Italy, 2021, pp. 1-7.

[5] S. Thangavel, D. Mohanraj, T. Girijaprasanna, S. Raju, C. Dhanamjayulu and S. M. Muyeen, "A Comprehensive Review on Electric Vehicle: Battery Management System, Charging Station, Traction Motors," *IEEE Access*, vol. 11, pp. 20994-21019, 2023.

[6] X. Yuan, S. Zhang, C. Zhang, A. Galassini, G. Buticchi and M. Degano, "Improved Model Predictive Current Control for SPMSM Drives Using Current Update Mechanism," *IEEE Trans. Ind. Electron.*, vol. 68, no. 3, pp. 1938-1948, Mar. 2021.

[7] W. Xie, X. Wang, F. Wang, W. Xu, R. M. Kennel, D. Gerling and R. D. Lorenz, "Finite-Control-Set Model Predictive Torque Control With a Deadbeat Solution for PMSM Drives," *IEEE Trans. Ind. Electron.*, vol. 62, no. 9, pp. 5402-5410, Sept. 2015.

[8] W. Xu, J. Zou, Y. Liu and J. Zhu, "Weighting Factorless Model Predictive Thrust Control for Linear Induction Machine," *IEEE Trans. Power Electron.*, vol. 34, no. 10, pp. 9916-9928, Oct. 2019.

[9] Y. Zhang and H. Yang, "Two-Vector-Based Model Predictive Torque Control Without Weighting Factors for Induction Motor Drives," *IEEE Trans. Power Electron.*, vol. 31, no. 2, pp. 1381-1390, Feb. 2016.

[10] S. Kouro, P. Cortes, R. Vargas, U. Ammann, and J. Rodriguez, "Model predictive control—a simple and powerful method to control power converters," *IEEE Trans. Ind. Electron.*, vol. 56, no. 6, pp. 1826-1838, 2009.

[11] C. Xu, Z. Han and S. Lu, "Deadbeat Predictive Current Control for Permanent Magnet Synchronous Machines With Closed-Form Error Compensation," *IEEE Trans. Power Electron.*, vol. 35, no. 5, pp. 5018-5030, May 2020.

[12] Y. Zhou, S. Zhang, C. Zhang, X. Li, X. Li and X. Yuan, "Current Prediction Error Based Parameter Identification Method for SPMSM With Deadbeat Predictive Current Control," *IEEE Trans. Energy Convers.*, vol. 36, no. 3, pp. 1700-1710, Sept. 2021.

[13] H. Fang, X. Duan, Y. Yang, Y. Wang and G. Luo, "Deadbeat Control of Permanent Magnet Synchronous Motor Based on MRAS Parameter Identification," in *2020 23rd Int. Conf. Electr. Mach. Syst. (ICEMS)*, Hamamatsu, Japan, 2020, pp. 161-166.

[14] K. Yin, L. Gao, W. Fu and Z. Feng, "Deadbeat Predictive Current Control of PMSM with Nonlinear Parameters Online Identification," in *2021 IEEE Int. Conf. Electron. Technol. (ICET)*, Chengdu, China, 2021, pp. 138-142.

[15] Y. Xu, S. Li and J. Zou, "Integral Sliding Mode Control Based Deadbeat Predictive Current Control for PMSM Drives With Disturbance Rejection," *IEEE Trans. Power Electron.*, vol. 37, no. 3, pp. 2845-2856, Mar. 2022.

[16] B. Wang, Z. Dong, Y. Yu, G. Wang and D. Xu, "Static-Errorless Deadbeat Predictive Current Control Using Second-Order Sliding-Mode Disturbance Observer for Induction Machine Drives," *IEEE Trans. Power Electron.*, vol. 33, no. 3, pp. 2395-2403, Mar. 2018.

[17] Y. Jiang, W. Xu, C. Mu and Y. Liu, "Improved Deadbeat Predictive Current Control Combined Sliding Mode Strategy for PMSM Drive System," *IEEE Trans. Veh. Technol.*, vol. 67, no. 1, pp. 251-263, Jan. 2018.

[18] K. Yu and Z. Wang, "Improved Deadbeat Predictive Current Control of Dual Three-Phase Variable-Flux PMSM Drives With Composite Disturbance Observer," *IEEE Trans. Power Electron.*, vol. 37, no. 7, pp. 8310-8321, July 2022.

[19] X. Zhang, B. Hou and Y. Mei, "Deadbeat Predictive Current Control of Permanent-Magnet Synchronous Motors with Stator Current and Disturbance Observer," *IEEE Trans. Power Electron.*, vol. 32, no. 5, pp. 3818-3834, May 2017.

[20] X. Yuan, S. Zhang and C. Zhang, "Enhanced Robust Deadbeat Predictive Current Control for PMSM Drives," *IEEE Access*, vol. 7, pp. 148218-148230, 2019.

[21] X. Yuan, S. Xie, J. Chen, S. Zhang, C. Zhang and C. H. T. Lee, "An Enhanced Deadbeat Predictive Current Control of SPMSM With Linear Disturbance Observer," *IEEE Trans. Emerg. Sel. Topics Power Electron.*, vol. 10, no. 5, pp. 6304-6316, Oct. 2022.

[22] L. He, F. Wang, J. Wang and J. Rodríguez, "Zynq Implemented Luenberger Disturbance Observer Based Predictive Control Scheme for PMSM Drives," *IEEE Trans. Power Electron.*, vol. 35, no. 2, pp. 1770-1778, Feb. 2020.

[23] F. Wang, D. Ke, X. Yu and D. Huang, "Enhanced Predictive Model Based Deadbeat Control for PMSM Drives Using Exponential Extended State Observer," *IEEE Trans. Ind. Electron.*, vol. 69, no. 3, pp. 2357-2369, March 2022.

[24] T. Türker, U. Buyukkeles and A. F. Bakan, "A Robust Predictive Current Controller for PMSM Drives," *IEEE Trans. Ind. Electron.*, vol. 63, no. 6, pp. 3906-3914, Jun. 2016.

[25] H. Le-Huy, K. Slimani and P. Viarouge, "Analysis and implementation of a real-time predictive current controller for permanent-magnet synchronous servo drives," *IEEE Trans. Ind. Electron.*, vol. 41, no. 1, pp. 110-117, Feb. 1994.

[26] Y. Zhang, J. Jin and L. Huang, "Model-Free Predictive Current Control of PMSM Drives Based on Extended State Observer Using Ultralocal Model," *IEEE Trans. Ind. Electron.*, vol. 68, no. 2, pp. 993-1003, Feb. 2021.

[27] Y. Zhang, W. Shen and H. Yang, "An Improved Deadbeat Predictive Current Control of PMSM Drives Based on the Ultra-local Model," *Chinese J. Electr. Eng.*, vol. 9, no. 2, pp. 27-37, Jun. 2023.